Determination of the Orbit of Asteroid 138846 (2000 VJ61) with the Methods of Gauss and Laplace

Odelia Lorch, Yunfei Ma, and Elaine Zhu

30 July 2017

Summer Science Program, University of Colorado Boulder 2017

Abstract

The purpose of this study is to determine the orbit of Near-Earth Asteroid 138846 (2000 VJ61). Orbital elements are calculated using the Gaussian and Laplacian methods with observations taken from 05 July 2017 to 24 July 2017. The Gaussian method is found to be more accurate than the Laplacian method. The asteroid is predicted to approach Earth most closely in July 2020, at a distance of $5.6 * 10^6$ km. The observations contribute to a large body of Near-Earth Asteroid data and provide the scientific community with a more accurate picture of Earth's celestial environment.

Table 1: Classical orbital elements as calculated using the Gaussian method

semi-major axis (a)	**AU**	2.200 ± 0.007
eccentricity (e)		0.565 ± 0.003
inclination (i)	$^\circ$	18.724 ± 0.047
longitude of ascending node (Ω)	$^\circ$	270.558 ± 0.038
argument of perihelion (ω)	$^\circ$	280.717 ± 0.263
true anomaly (ν)	$^\circ$	90.301 ± 0.614

1 Introduction

Since the 1801 discovery of Ceres, the scientific community has grown increasingly aware of the asteroids in the Solar System, and the determination of their orbits has become an extensive task. At first, astronomical technology limited discoveries to asteroids in the Main Asteroid Belt. In the late nineteenth century, however, asteroids within the Inner Solar

System, deemed Near-Earth Asteroids (NEAs), became detectable. With the rise of digital processing in the last few decades, the rate of asteroid discovery increased exponentially. As of July 2017, over 16,000 NEAs have been discovered. [2].

The close proximity of NEAs draws attention for several reasons. First, an awareness of the locations of NEAs provides a more accurate picture of Earth's nearby environment, making it safer and easier to plan and navigate space missions. Second, knowing the locations of these neighboring objects allows for potential missions to extract surface samples, by which we can learn more about the origin and evolution of our Solar System [7]. Lastly, NEAs pose a threat of collision with Earth, making awareness of their orbits critical for the safety of humanity.

It is difficult to reliably predict the orbit of an asteroid far into the future, as its path is continuously altered by the forces in its environment. As it interacts with the Solar System, it becomes a part of a large N-body problem [3], affected by somewhat unpredictable gravitational forces and collisions. Therefore, in order to keep track of NEAs, their orbits must be recalculated regularly.

While the calculation of classical orbital elements from the position and velocity of an asteroid is relatively simple, its position and velocity cannot be calculated analytically; rather, they must be found using numerical methods. Two of the most prominent classical methods are those of Pierre-Simon Laplace and Carl F. Gauss [4], which favor different orbits.

Asteroid 2000 VJ61 was discovered in the year 2000 and is considered a NEA with a semi-major axis of 2.2 AU [5]. In this report, the Gaussian and Laplacian methods are utilized and compared in their determination of the asteroid's position, velocity, and orbital elements in order to find an accurate characterization of its orbit for the foreseeable future.

2 Methods

2.1 Collection of Data

The PlaneWave Instruments 20-inch CDK f/6.8 telescope and Diffraction Limited STF-8300M camera at the University of Colorado Boulder were used for observations. Observational data were taken on four separate occasions: 05 July 2017, 09 July 2017, 16 July 2017, and 24 July 2017.

2.2 Processing of Data

The light frames were processed using standard methods. Astrometry and photometry were then performed on the processed images. Using the celestial and CCD pixel coordinates of

several reference stars, code that implemented the Least Squares Plate Reduction (LSPR) method was utilized to compute and extrapolate the transformation to determine the asteroid's celestial coordinates from its CCD pixel coordinates. Similarly, the asteroid's magnitude was determined with reference to several surrounding stars that were used to calibrate the magnitude in the images.

With the right ascension (RA) and declination (Dec) of the asteroid, time of each observation, and Sun-Earth vector as found on the JPL Horizons database [5], code that implemented the Gaussian orbit determination method was used to generate an initial guess and subsequent iterations for the position ($\vec{r}$) and velocity ($\dot{\vec{r}}$) vectors of the asteroid. The Laplacian orbit determination method was likewise implemented.

These results were checked in two ways. First, the calculated orbital elements were compared to those in the JPL Horizons database [5]. Second, code was used that generated an ephemeris of the celestial coordinates of the asteroid from its orbital elements, and the results were compared to the original celestial coordinates calculated with astrometry.

To determine the risk of possible collision of 2000 VJ61 with Earth, the asteroid's position as a function of time was treated as a central-force problem, with the Sun being the gravitational center. With code that modeled this problem and used Newton's Second Law and Universal Gravitation, both the asteroid's and Earth's position and velocity were numerically integrated 100 years forward in time. The code found the time, date, and distance of the asteroid's closest encounter with Earth in the next century.

2.3 Calculation of Uncertainty

The standard deviation of the residuals of each reference star used in the astrometry process was taken as the uncertainty in the calculated position and velocity vectors of the asteroid at each observation. Uncertainty in the photometric data for each observation was taken as the standard error in the magnitude of the asteroid in each stacked photo of the observation. Uncertainty in the orbital elements was determined using the standard Jackknife uncertainty method. The four data points were divided into four combinations of three, and each triplet was used to calculate the orbital elements once. The standard error of the four values of each element was taken to be the uncertainty.

3 Results

3.1 Observational Data

The asteroid's RA and Dec were calculated using LSPR, and its magnitude was calculated using standard photometric procedures. The reference stars used in both of these processes

are labeled in red, and the asteroid is labeled in blue. (*Figures 1-4*).

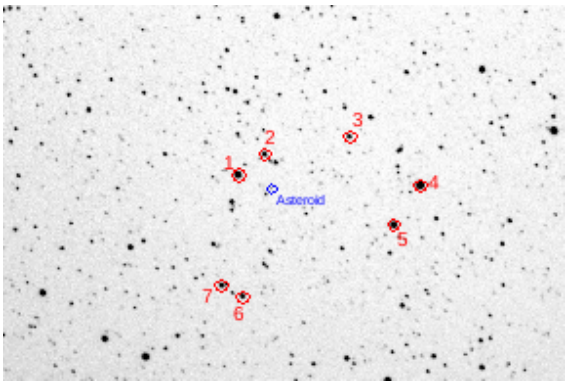

Figure 1: CCD Image from Observation 1

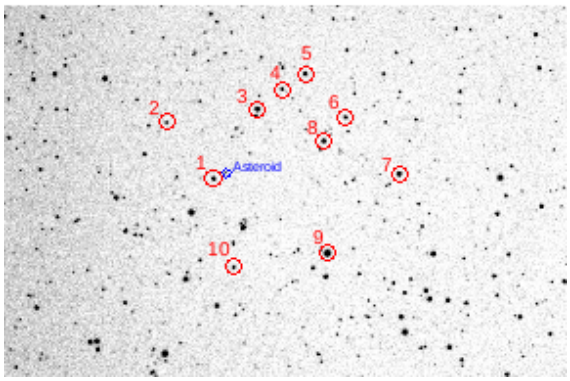

Figure 2: CCD Image from Observation 2

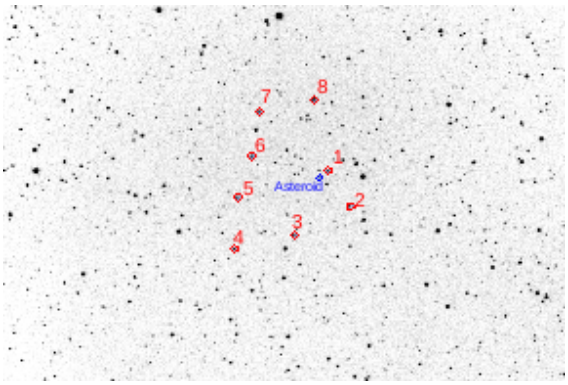

Figure 3: CCD Image from Observation 3

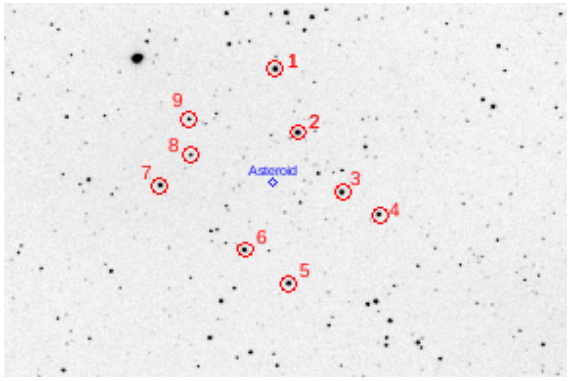

Figure 4: CCD Image from Observation 4

Astrometry and photometry produced the following results for each observation. Additionally, the signal-to-noise ratio of the asteroid was found in the CCD image used for astrometry of each observation.

Table 2: Summary of astrometry and photometry for each observation

Observation		**1**	**2**	**3**	**4**
Time	**JD**	2457939.7638	2457943.6986	2457950.7277	2457958.7291
	HMS	6:19:48.09 (05 July 2017)	04:45:59.98 (09 July 2017)	05:27:50.84 (16 July 2017)	5:29:54.90 (24 July 2017)
Right ascension	**HMS**	17:23:59.4337	17:24:13.676	17:25:52.5125	17:29:24.8516
	degrees	260.9976 ± 0.0006	261.0570 ± 0.0002	261.4688 ± 0.0007	262.3535 ± 0.0002
Declination	**DMS**	-16°32' 6.1674"	-14°48' 47.3867"	-12°31' 59.4093"	-10°50' 41.5704"
	degrees	-16.53505 ± 0.00007	-14.81326 ± 0.0003	-12.5332 ± .00226	-10.8449 ± 0.00003
rMag		16.104 ± 0.3072	16.22 ± 0.1503	16.8580 ± 0.0323	17.469 ± 0.1372
Signal-to-Noise ratio		56.635	40.248	54.929	24.605

3.2 Gaussian Results

The Gaussian method was used to calculate the light-corrected time, position and velocity vectors of the asteroid, and its classical orbital elements. Light-travel time from the asteroid to Earth is accounted for in order to refine the data. Accompanying each value in the following table is the corresponding uncertainty as determined by the Jackknife uncertainty method.

Table 3: Gaussian method results with uncertainties

light-corrected time (t)	**JD**	2457948.335
position vector ($\vec{r}$)	**AU**	$< 0.298, -1.410, 0.077 >$
velocity vector ($\dot{\vec{r}}$)	**AU**	$< 0.8445, 0.2956, 0.2847 >$
semi-major axis (a)	**AU**	1.956 ± 0.054
eccentricity(e)		0.490 ± 0.023
inclination (i)	$^\circ$	17.835 ± 0.707
longitude of ascending node (Ω)	$^\circ$	270.446 ± 1.714
argument of perihelion(ω)	$^\circ$	268.678 ± 8.252
true anomaly (ν)	$^\circ$	97.403 ± 6.810

3.3 Comparison of Ephemeris Generation and Astrometry

The RAs and Decs of the asteroid for the 16 July observation were calculated with LSPR. In the following table, those values are compared to the RAs and Decs calculated with the ephemeris generation code from the Gaussian orbital elements.

Table 4: Comparison of celestial coordinates of the asteroid during observation 4

	LSPR	**Ephemeris generation**	**Percent error**
RA	17:29:24.8516	17: 29: 31.1359	0.0001%
dec	-10°50' 41.5704"	-10°50' 21.0850"	0.0005%

3.4 Laplacian Results

The Laplacian method of orbit determination was used in addition to the Gaussian method to calculate the light-corrected time, position and velocity vectors of the asteroid, and its classical orbital elements (*Table 3*).

Table 5: Laplacian method results with uncertainties

light-corrected time (t)	**JD**	2457947.2087
position vector ($\vec{r}$)	**AU**	$< 0.2680, 1.5072, 0.0942 >$
velocity vector ($\dot{\vec{r}}$)	**AU**	$< 0.8311, 0.2851, 0.3086 >$
semi-major axis (a)	**AU**	2.3014 ± 0.0159
eccentricity(e)		0.5592 ± 0.0259
inclination (i)	$^\circ$	20.4337 ± 0.7190
longitude of ascending node (Ω)	$^\circ$	270.4940 ± 0.2800
argument of perihelion(ω)	$^\circ$	283.4583 ± 2.7816
true anomaly (ν)	$^\circ$	86.7658 ± 3.6886

3.5 Comparison to JPL Ephemerides

To check the results of the Gaussian and Laplacian methods against a third, reliable reference, the results were compared to the JPL Horizons database. In the following table are the orbital element values generated by JPL Horizons, the Gaussian and Laplacian results, and their respective percent deviations from the JPL values. The Gaussian method produced values that were more consistent with JPL Horizons, with percent errors of approximately 0.1% or less.

Table 6: Gaussian and Laplacian results compared to JPL Horizons Ephemerides

		JPL Horizons	**Gaussian Method**	**Percent error**	**Laplacian Method**	**Percent error**
semi-major axis (a)	**AU**	2.1847	2.1875 ± 0.0012	0.1282%	2.3014 ± 0.0159	5.3417%
eccentricity (e)		0.5631	0.5638 ± 0.0003	0.0124%	0.5592 ± 0.0259	0.6926%
inclination (i)	$^\circ$	18.6776	18.6912 ± 0.0054	0.0038%	20.4337 ± 0.7190	9.4022%
longitude of ascending node (Ω)	$^\circ$	270.5805	270.5842 ± 0.0026	0.0014%	270.4940 ± 0.2800	0.0320%
argument of perihelion (ω)	$^\circ$	280.4800	280.4736 ± 0.0221	0.0023%	283.4583 ± 2.7816	1.0619%
true anomaly (ν)	$^\circ$	90.0973	90.0654 ± 1.1150	0.0354%	86.7658 ± 3.6886	3.6977%

3.6 Extrapolation of Asteroid and Earth Positions

Both the asteroid's and Earth's positions were numerically integrated forward into time. The integration calculated that the asteroid's closest distance from Earth in the next 100 years will occur in July 2020 at a distance of 0.037 AU.

4 Analysis

As is evident in the Gaussian (*Table 3*) and Laplacian results (*Table 5*), the uncertainties are smaller with the Gaussian method; therefore it is the method that works more precisely

with the data. Furthermore, the Gaussian method is more consistent with values previously determined by JPL Horizons (*Table 6*). In addition, when orbital elements from the Gaussian method are used to calculate the celestial coordinates, the deviations from the original values are very small (*Table 4*). The Gaussian method works better than the Laplacian method for several reasons.

First, the intervals of time between observations are not evenly spaced. Because the Laplacian Method requires the same length of time in between each observation [4], this method does not produce the most accurate results for our observational data. The Gaussian method is more flexible with non-uniform time intervals, which made it the optimal method to use for the orbit determination in this case.

However, the Gaussian method has limits as well. The Gaussian method initially approximates sectors of the orbit as triangles; if the arcs are too curved or large, the truncated sections become significant. Although the Gaussian method corrects for this by means of iterations of the f- and g-series, the radius of convergence of these series decreases for more eccentric elliptical orbits [1]. In the case of 2000 VJ61 with an eccentricity of 0.56, the position vector is able to converge to 10^{-9} AU in magnitude, indicating that the orbit is not too eccentric for the Gaussian method. Because the Laplacian method also fails when the orbit has such small eccentricity that its orbit is extrapolated to a more linear shape, this is another reason the Gaussian method is more favorable for 2000 VJ61's orbit.

Several sources of error were present in the project. Deviation from standard methods occurred on the first observation, when flat-dark frames were not taken to calibrate the flat-field frames. Without this calibration, noise levels were not fully corrected for, which likely introduced error into the astrometry. The signal-to-noise ratio for the 24 July observation was 24.6, a relatively low value, because of its predicted high magnitude on that date. Thus, the centroid positions of the asteroid on the CCD for that observation had significant uncertainty.

The numerical integration of the positions of Earth and the asteroid is sensitive to the small deviations that accumulate with each iteration. It is not known how large this deviation is for the predicted nearest approach. In addition, the numerical integration takes into account only the gravitational force of the Sun, ignoring the gravitational forces of other Solar System bodies.

The method of Least Squares Plate Reduction computes a linear transformation between CCD coordinates and celestial coordinates. In reality, the relationship is not linear, as the CCD is planar while the celestial sphere is not. This approximation is sufficient for the small range of view presented on the CCD, but it can still introduce errors.

The magnitude calculations were also subject to errors. The reference star method of photometry assumes that CCD response to photons is linear when in fact they are not. Thus, the calculated magnitudes, some corresponding to intensities 100 times as weak as the reference star, could be inaccurate. Moreover, the magnitude of an irregularly-shaped body, such as an asteroid, may not be precisely constant in the first place; the intensity depends on surface area, which depends on the orientation of the asteroid in space.

5 Conclusion

With four observations in the span of one month, the classical orbital elements of 138846 VJ61 were calculated using both the Gaussian and Laplacian methods. The Gaussian method proved to be more accurate in this case, with values less than 1% away from those of JPL. Numerical extrapolation of the asteroid's position into the next century resulted in a closest approach of over $5 * 10^6$ km. It is safe to conclude that 2000 VJ61 will not collide with Earth in the foreseeable future. To further the accuracy of the determined orbit, this study can be expanded with more data from a greater number of observations and a variety of locations.

6 Acknowledgements

We would like to thank our professors, Dr. Michael Dubson and Dr. Tracy Furutani, for their help and guidance throughout our project. Additionally, we are grateful to our teacher assistants, Jonathan Joo, Lindsey Whitesides, Tanay Bhandarkar, and Cyndia Cao for their patience and advice during our observations. Finally, we would like to thank the University of Colorado Boulder for providing the facilities and technology we used in our research.

References

[1] Branham, R. (2003). Laplacian Orbit Determination. ADeLA2002 - Astronomy In Latin America, 1(1), 85-90.

[2] Discovery Statistics. (2017). cneos.jpl.nasa.gov. Retrieved 30 July 2017, from https://cneos.jpl.nasa.gov/stats/totals.html

[3] Heggie, D. (2005). The Classical Gravitational N-Body Problem (pp. 1-18). Cornell University Library. Retrieved from https://arxiv.org/pdf/astro-ph/0503600.pdf

[4] Herrick, S. (1937). On the Laplacian and Gaussian Orbit Methods. Publications Of The Astronomical Society Of The Pacific, 49(287), 17.

[5] HORIZONS Web-Interface. (2017). ssd.jpl.nasa.gov. Retrieved 30 July 2017, from https://ssd.jpl.nasa.gov/horizons.cgi

[6] Klokacheva, M. (1991). Determination of a Preliminary Orbit by the Laplace Method. Soviet Astronomy, 35(4), 428.

[7] Northon, K. (2016). NASA Prepares to Launch First U.S. Asteroid Sample Return Mission. NASA. Retrieved 30 July 2017, from https://www.nasa.gov/press-release/nasa-prepares-to-launch-first-us-asteroid-sample-return-mission

7 Appendices

7.1 Appendix 1: Observational Methods

Table 7: Overview of observational methods

Observation	1	2	3	4
Date	05 July 2017	09 July 2017	16 July 2017	24 July 2017
Binning	1x1	1x1	1x1	1x1
Exposure time	80 seconds	60 seconds	75 seconds	80 seconds
Series quantity	5 images	5 images	5 images	5 images

7.2 Appendix 2: Astrometry and Photometry

Table 8: Observation 1 (05 July 06:19:48 UT)

Object	**x (pix)**	**y (pix)**	**RA (deg)**	**DEC (deg)**	**rmag**
Star 1	1309.258	1224.047	260.9916474	-16.5191334	10.6
Star 2	1448.891	1114.208	260.9805645	-16.5309728	12.6
Star 3	1896.271	1017.415	260.9692403	-16.5706239	12.9
Star 4	2269.000	1279.739	260.9917027	-16.6054103	09.9
Star 5	2130.378	1493.949	261.0124724	-16.5940414	10.9
Star 6	1332.784	1878.199	261.0526489	-16.5244395	11.7
Star 7	1223.706	1820.474	261.0477824	-16.5145231	12.3
Asteroid	1483.204	1298.350	260.997641 (0.000043)	-16.535047 (0.000070)	16.1 (0.2)

Table 9: Observation 2 (09 July 04:46:00 UT)

Object	**x (pix)**	**y (pix)**	**RA (deg)**	DEC	rmag
Star 1	1401.025	1224.992	261.0598539	-14.8075470	13.6
Star 2	1157.532	929.521	261.0321036	-14.7856131	15.2
Star 3	1626.250	858.309	261.0255459	-14.8281370	13.0
Star 4	1755.413	753.767	261.0158124	-14.8398325	14.6
Star 5	1874.664	673.182	261.0083018	-14.8506609	13.5
Star 6	2082.587	902.396	261.0299289	-14.8694995	14.1
Star 7	2360.162	1200.411	261.0578524	-14.8945014	12.9
Star 8	1969.805	1026.918	261.0414848	-14.8591970	13.1
Star 9	1988.810	1617.441	261.0968209	-14.8607287	11.5
Star 10	1504.250	1690.712	261.1035359	-14.8167539	14.5
Asteroid	1462.633	1194.100	261.056983 (0.000011)	-14.813163 (0.000022)	16.2 (0.1)

Table 10: Observation 3 (16 July 05:27:51)

Object	**x (pix)**	**y (pix)**	**RA (deg)**	**DEC (deg)**	**rmag**
Star 1	1792.013	1251.908	261.4656015	-12.5373667	14.2
Star 2	1905.372	1447.481	261.4834177	-12.5481495	15.5
Star 3	1606.43	1603.56	261.4986589	-12.5214267	15.1
Star 4	1288.593	1682.732	261.5067806	-12.4928114	15.4
Star 5	1301.786	1396.603	261.4802689	-12.4932659	15.0
Star 6	1381.688	1170.963	261.4591092	-12.4999606	14.7
Star 7	1491.799	923.592	261.4359886	-12.5028392	14.7
Star 8	1715.707	859.789	261.4293677	-12.5294287	13.0
Asteroid	1749.388	1285.497	261.468802281 (0.000046)	-12.5332 (0.0023)	6.9 (0.0)

Table 11: Observation 4 (24 July 05:29:55)

Object	**x (pix)**	**y (pix)**	**RA (deg)**	**DEC (deg)**	**rmag**
Star 1	1737.649	697.185	262.2970409	-10.842662	12.1
Star 2	1852.59	1032.386	262.3276177	-10.8539898	12.0
Star 3	2079.824	1346.644	262.3560198	-10.8753164	12.3
Star 4	2270.053	1463.295	262.3662545	-10.8928289	12.6
Star 5	1806.093	1828.857	262.4011227	-10.8516503	12.4
Star 6	1577.551	1651.084	262.3853356	-10.8305495	12.6
Star 7	1145.855	1310.289	262.3550109	-10.790607	12.7
Star 8	1302.269	1150.773	262.3399586	-10.8044095	13.8
Star 9	1293.827	962.501	262.3226174	-10.8031625	14.2
Asteroid	1744.966	1310.744	262.353548 0.000016)	-10.844881 (0.000033)	17.5 (0.1)

7.3 Appendix 3: Iterations

Table 12: Gaussian iterations of position and velocity for the combination of observations 1, 2, 3

Iteration	**Position vector** ($\vec{r_0}$)	**Velocity vector** ($\dot{\vec{r_0}}$)
initial guess	$< 0.210430, -1.437752, -0.532800 >$	$< 0.833489, -0.527611, 0.138321 >$
1	$< 0.217887, -1.390695, -0.520200 >$	$< 0.842736, -0.459515, 0.136221 >$
2	$< 0.220896, -1.371571, -0.515080 >$	$< 0.846450, -0.431838, 0.135353 >$
3	$< 0.222230, -1.363098, -0.512812 >$	$< 0.848096, -0.419574, 0.134970 >$
4	$< 0.222842, -1.359205, -0.511770 >$	$< 0.848853, -0.413937, 0.134794 >$
5	$< 0.223128, -1.357387, -0.511283 >$	$< 0.849206, -0.411304, 0.134712 >$
6	$< 0.223263, -1.356531, -0.511054 >$	$< 0.849373, -0.410065, 0.134673 >$
7	$< 0.223327, -1.356127, -0.510945 >$	$< 0.849452, -0.409479, 0.134655 >$
8	$< 0.223357, -1.355935, -0.510894 >$	$< 0.849489, -0.409202, 0.134646 >$
9	$< 0.223371, -1.355845, -0.510870 >$	$< 0.849506, -0.409071, 0.134642 >$
10	$< 0.223378, -1.355802, -0.510858 >$	$< 0.849515, -0.409009, 0.134640 >$
11	$< 0.223381, -1.355781, -0.510853 >$	$< 0.849519, -0.408980, 0.134639 >$
12	$< 0.223383, -1.355772, -0.510850 >$	$< 0.849520, -0.408966, 0.134639 >$
13	$< 0.223383, -1.355767, -0.510849 >$	$< 0.849521, -0.408959, 0.134639 >$
14	$< 0.223384, -1.355765, -0.510849 >$	$< 0.849522, -0.408956, 0.134638 >$
15	$< 0.223384, -1.355764, -0.510848 >$	$< 0.849522, -0.408954, 0.134638 >$
16	$< 0.223384, -1.355764, -0.510848 >$	$< 0.849522, -0.408954, 0.134638 >$
17	$< 0.223384, -1.355763, -0.510848 >$	$< 0.849522, -0.408953, 0.134638 >$
18	$< 0.223384, -1.355763, -0.510848 >$	$< 0.849522, -0.408953, 0.134638 >$
19	$< 0.223384, -1.355763, -0.510848 >$	$< 0.849522, -0.408953, 0.134638 >$
20	$< 0.223384, -1.355763, -0.510848 >$	$< 0.849522, -0.408953, 0.134638 >$
21	$< 0.223384, -1.355763, -0.510848 >$	$< 0.849522, -0.408953, 0.134638 >$
22	$< 0.223384, -1.355763, -0.510848 >$	$< 0.849522, -0.408953, 0.134638 >$
23	$< 0.223384, -1.355763, -0.510848 >$	$< 0.849522, -0.408953, 0.134638 >$
24	$< 0.223384, -1.355763, -0.510848 >$	$< 0.849522, -0.408953, 0.134638 >$
25	$< 0.223384, -1.355763, -0.510848 >$	$< 0.849522, -0.408953, 0.134638 >$

Table 13: Laplacian iterations of position and velocity for the combination of observations 1, 2, 3

Iteration	**Position vector** ($\vec{r_0}$)	**Velocity vector** ($\dot{\vec{r_0}}$)
initial guess	$< 0.206110, -1.465623, -0.540258 >$	$< 0.832843, -0.455897, 0.176234 >$
1	$< 0.212207, -1.426880, -0.529886 >$	$< 0.835328, -0.432218, 0.165624 >$
2	$< 0.214604, -1.411646, -0.525808 >$	$< 0.836389, -0.422375, 0.161594 >$
3	$< 0.215613, -1.405236, -0.524092 >$	$< 0.836850, -0.418137, 0.159924 >$
4	$< 0.216049, -1.402463, -0.523349 >$	$< 0.837052, -0.416287, 0.159207 >$
5	$< 0.216240, -1.401249, -0.523024 >$	$< 0.837142, -0.415473, 0.158894 >$
6	$< 0.216324, -1.400715, -0.522882 >$	$< 0.837181, -0.415114, 0.158756 >$
7	$< 0.216361, -1.400480, -0.522819 >$	$< 0.837198, -0.414956, 0.158695 >$
8	$< 0.216377, -1.400376, -0.522791 >$	$< 0.837206, -0.414886, 0.158669 >$
9	$< 0.216385, -1.400330, -0.522778 >$	$< 0.837209, -0.414855, 0.158657 >$
10	$< 0.216388, -1.400310, -0.522773 >$	$< 0.837211, -0.414842, 0.158652 >$
11	$< 0.216389, -1.400301, -0.522771 >$	$< 0.837212, -0.414836, 0.158649 >$
12	$< 0.216390, -1.400297, -0.522770 >$	$< 0.837212, -0.414833, 0.158648 >$
13	$< 0.216390, -1.400295, -0.522769 >$	$< 0.837212, -0.414832, 0.158648 >$
14	$< 0.216390, -1.400295, -0.522769 >$	$< 0.837212, -0.414831, 0.158648 >$
15	$< 0.216390, -1.400294, -0.522769 >$	$< 0.837212, -0.414831, 0.158648 >$
16	$< 0.216390, -1.400294, -0.522769 >$	$< 0.837212, -0.414831, 0.158648 >$
17	$< 0.216390, -1.400294, -0.522769 >$	$< 0.837212, -0.414831, 0.158648 >$
18	$< 0.216390, -1.400294, -0.522769 >$	$< 0.837212, -0.414831, 0.158648 >$
19	$< 0.216390, -1.400294, -0.522769 >$	$< 0.837212, -0.414831, 0.158648 >$
20	$< 0.216390, -1.400294, -0.522769 >$	$< 0.837212, -0.414831, 0.158648 >$
21	$< 0.216390, -1.400294, -0.522769 >$	$< 0.837212, -0.414831, 0.158648 >$
22	$< 0.216390, -1.400294, -0.522769 >$	$< 0.837212, -0.414831, 0.158648 >$
23	$< 0.216390, -1.400294, -0.522769 >$	$< 0.837212, -0.414831, 0.158648 >$